Soft Supracrystals of Au Nanocrystals with Tunable Mechanical Properties

*Cong Yan, Imad Arfaoui, Nicolas Goubet, and Marie-Paule Pileni**

The elastic properties of highly ordered three-dimensional colloidal crystals of gold nanocrystals (called supracrystals) are reported. This study is based on the simultaneous growth of two kinds of gold nanocrystal supracrystals that range in size from 5 nm to 8 nm: interfacial supracrystals and precipitated supracrystals. The elastic properties are deduced from nanoindentation measurements performed with an atomic force microscope. The Young's modulus of the interfacial supracrystals, which grow layer-by-layer and form well-defined films, is compared to that of precipitated supracrystals, which are produced by homogeneous growth in solution. For the precipitated supracrystals, characterized by a thickness larger than 1 μm, the Oliver and Pharr model is used to determine the elastic moduli, which are in the gigapascal range and decrease with increasing nanocrystal size. For the interfacial supracrystals, with 300 nm average thickness, a second model (plate model) is applied in addition to the Oliver and Pharr model. These two models confirm independently that the interfacial films are very soft with Young's modulus in the range of 80–240 MPa. This result reveals a totally new feature of nanocrystal solids, never emphasized before. It is shown that these changes in the Young's modulus are related to the supracrystal growth mechanism.

1. Introduction

In the last 15 years,[1–8] self-assemblies of 3D superlattices of inorganic (semiconductor, metal, oxide, etc.) nanometer-sized particles (2–10 nm) have been produced and intensely studied. These assemblies are called supracrystals or supercrystals and show crystalline structures as observed for bulk materials. All these suprastructures induce different collective properties,[7] with unique and tunable vibrational, photoluminescent, electronic, and magnetic properties.[9–17] They are potentially strong candidates for novel artificial solids.[7,9–11,13,18–22] Meanwhile, cutting-edge technology is looking for flexible and bendable components for the next generation of electronics,[23] circuits,[24] and devices[25] to replace and enhance the performance of the current organic ones.[23] Colloidal supracrystals could be highly competitive candidates but require specific mechanical properties.

Dr. C. Yan, Dr. I. Arfaoui, N. Goubet, Prof. M.-P. Pileni
Laboratoire des Matériaux Mésoscopiques et Nanométriques
University Pierre & Marie Curie
BP 52, 4 Place Jussieu, 75005 Paris, France
E-mail: marie-paule.pileni@upmc.fr

DOI: 10.1002/adfm.201202563

Until now, only a few systematic studies of the mechanical properties of these supracrystals, which are of great importance in determining their application areas, have been published. It was found that by applying a magnetic field perpendicular to the substrate during the evaporation of Co colloidal solution, well-defined columns of Co nanocrystals (NCs) were produced, either in the form of hexagonal networks, when supracrystals are observed, or labyrinths, for disordered aggregates.[26] These changes in the patterns were explained in terms of mechanical properties. The mechanical properties of nanometer-scale materials are mostly studied using a nanoindentor or atomic force microscopy (AFM), whereby the latter is becoming more and more popular. One example is the AFM studies of the elastic modulus of the transparent nanorod, which exhibits a much larger value of Young's modulus than other nanostructures.[27] In the field of nanocrystal supracrystals, considerable attention is focused on the mechanical properties of Au nanocrystals, owing to their versatile structures[28] and properties.[29] Mueggenburg et al.[30] studied Au NC monolayers and found a Young's modulus on the order of gigapascals; Tam et al.[31] performed nanoindentation studies of well-ordered NC supracrystals composed of 7 nm PbS NCs stabilized with oleic acid ligands, where the mechanical properties are attributed to the organic capping agents surrounding the inorganic core. Podsiadlo et al.[12] studied both the shaped supracrystals and the evaporated, layer-by-layer film supracrystals. They correlated the mechanical properties of PbS, CdSe, and $CoPt_3$ supercrystals with the NC size, capping ligands, and degree of ordering. However, in almost all of these studies it was found that the supracrystals have Young's modulus on the order of several gigapascals, which is far from soft, and not suitable to satisfy the desire for flexible and bendable inorganic materials.

Here, we report one type of soft supracrystal as well as its simutaneously grown counterpart supracrystal. We measured and discuss the mechanical properties of NC films (or interfacial supracrystals) and shaped supracrystals (or precipitated supracrystals) differing in their growth mechanism. For this purpose, we used the Oliver and Pharr model to determine the elastic modulus *E*. However, since the interfacial supracrystals have a thickness around 300 nm, which could be a limitation for applying the Oliver and Pharr model, we adapted and used

another model — the plate model. Both models confirm that the *E* values for the interfacial supracrystals lie in the range 100–200 MPa, which indicates that these supracrystals can be considered as soft materials. Moreover, we compared the Young's moduli of interfacial supracrystals to those of precipitated supracrystals, as well as supracrystal films obtained through evaporation, which clearly demonstrated a change in the elastic properties with the supracrystal growth mechanism.

2. Results and Discussion

2.1. Gold Nanocrystal Supracrystal Synthesis

Gold NCs with low size distribution (<7%) and various sizes (5, 6, 7, and 8 nm) were prepared and dispersed in toluene.[32] For simplicity we refer to them as Au_5, Au_6, Au_7, and Au_8, respectively. Supracrystals are produced by means of two simultaneous growth processes, which are described elsewhere.[29] In brief, when the colloidal solution is kept for at least 7 days in saturated toluene atmosphere, a film appears at the air/toluene interface and simultaneously aggregated precipitates are observed at the bottom of the beaker. A careful characterization shows that they have a face-centered cubic (fcc) structure. The film is produced layer-by-layer, which floats at the air/toluene interface. The precipitated supracrystals, which result from a homogeneous supracrystal growth, lie at the bottom of the beaker. That is why these two types of supracrystals are referred to as interfacial and precipitated supracrystals, respectively. For each type of supracrystal and each nanocrystal size, we deduced the Young's modulus from the nanoindentation measurements.

2.2. Interfacial Supracrystals

In **Figure 1**, the scanning electron microscopy (SEM) image (Figure 1a) shows that the interfacial supracrystals are of constant thickness and consist of highly ordered NCs with a long coherence length (more than a few micrometers). The high-resolution SEM (HRSEM) image (Figure 1b) and AFM image (Figure 1c) present similar features, while straight edges are also observed as well as dislocations. In nanoindentation measurements, the thickness of the supracrystals should be at least 10 times the indentation depth in order to avoid effects from the substrate.[33] Since the interfacial supracrystals are about 300 nm thick and the indentation depths for our measurements are typically around 80 nm, usual substrates (e.g., Si wafers) are not appropriate. In practice, the interfacial supracrystals are deposited onto a transmission electron microscopy (TEM) grid with 2.6 μm diameter circular holes with center-to-center distance of

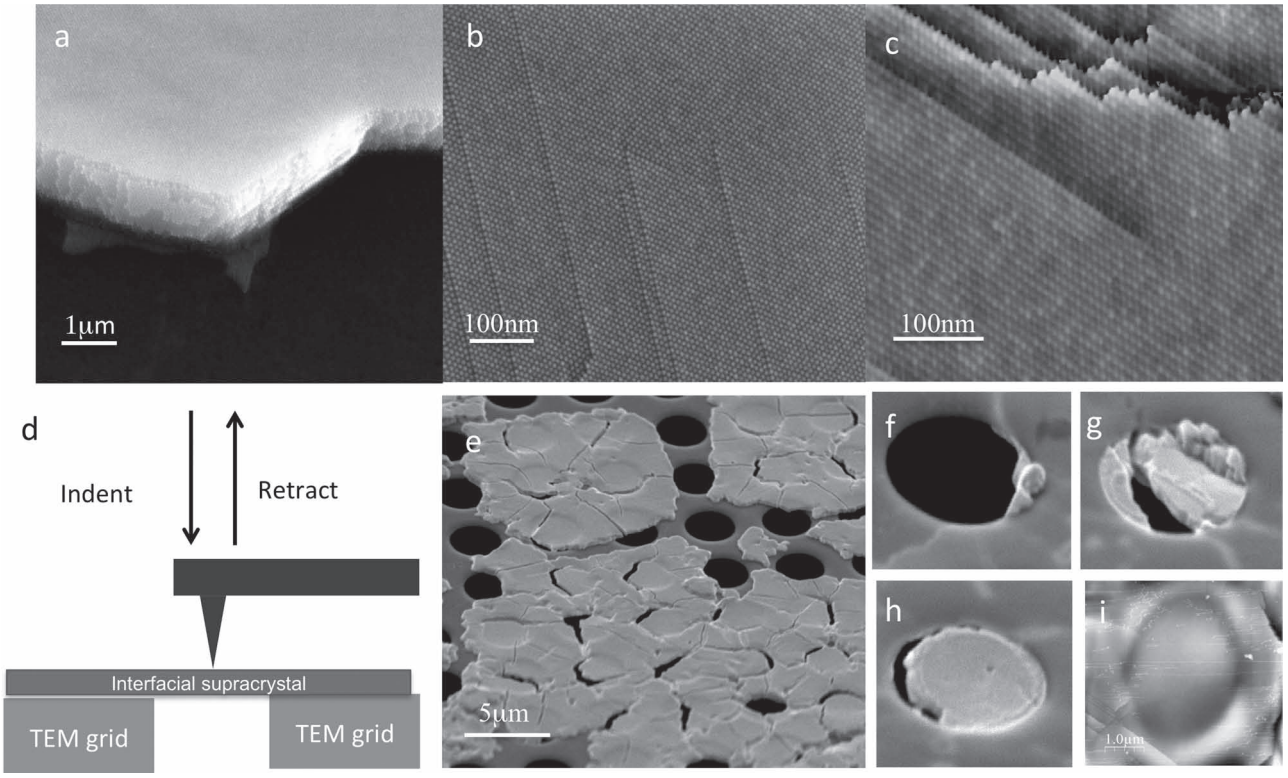

Figure 1. SEM and AFM images of interfacial Au supracrystals. a) Low-magnification SEM image of interfacial supracrystals showing constant thickness. b,c) High-magnification SEM image showing dislocations and the corresponding AFM image. d) Schematic illustration of nanoindentation measurements performed on freestanding interfacial supracrystals. e) SEM image of interfacial supracrystals on a TEM grid. f–h) SEM images of holes covered by freestanding interfacial supracrystals. i) Corresponding AFM image.

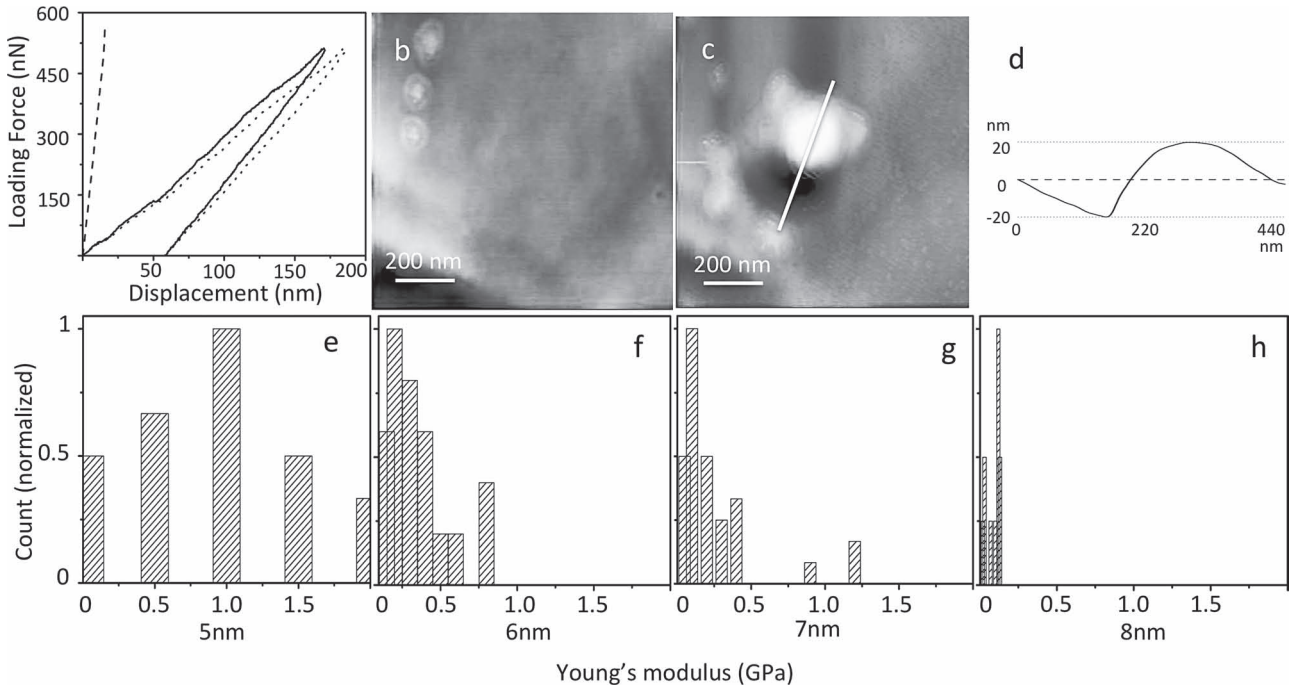

Figure 2. AFM nanoindentation performed on interfacial Au supracrystals. a) Force curve obtained during the indentation measurements. The dotted curve is the initial force curve (indenting and retracting) and is calibrated by the measurements on mica, the dashed curve. The solid curve is the final force curve resulting from the calibration and used to calculate the Young's modulus. b,c) AFM images recorded before (b) and after (c) the indentation. The residual mark clearly shows the pile of NCs. d) The profile of the residual mark; the height of the NC pile is almost the same as the depth of the residual mark. e–h) Histograms of Young's modulus obtained from interfacial supracrystals with different NC sizes (5 nm, 6 nm, 7 nm, 8 nm).

4 μm. The indentation is performed at the center of the freestanding films, as illustrated in Figure 1d. The cracks observed on the films by SEM (Figure 1e–h) are avoided during the measurements and a smooth freestanding film is always chosen for the nanoindentation measurements (inset of Figure 1i).

Figure 2a shows a typical force–displacement curve obtained from the measurements. AFM images were recorded before (Figure 2b) and after (Figure 2c) indentation. The residual mark is observed clearly (Figure 2c) and NCs are piled up next to it. Figure 2d displays the profile of the residual mark, from which it can be seen that the height of the NC pile is almost the same as the depth of the indentation mark. A number of measurements were performed at different spots for each sample and for each NC size of the interfacial supracrystals. Figure 2e–h display the corresponding histograms. **Table 1** shows that the Young's modulus of the interfacial supracrystals decreases from 1.1 GPa to 0.11 GPa when the NC size increases from 5 nm (Au_5) to 8 nm (Au_8). These values are rather low compared to those already published.[31] At this stage we need to evaluate the validity of the model used to deduce the elastic Young's moduli values. In fact, the Oliver and Pharr method is based on the assumption that the sample has infinite thickness, which is not the case here for the interfacial supracrystals. Moreover, the interfacial supracrystal may bend downwards under the pressure of the AFM cantilever. All these concerns raise the doubt that the Oliver and Pharr model, although widely used for measurements of supracrystal systems, may not be fully suitable in our case of measuring freestanding films of several hundred nanometer thickness. One possible solution is to use the models for ultrathin films,[34,35] but in these models a precondition is that the film displacement is significantly larger than the film's thickness, which is not the case in our measurements. Therefore, considering the physical conditions of our freestanding films, we introduce, for the first time, the plate model to determine the Young's modulus of freestanding interfacial supracrystal films.

In the plate model the film is treated as a flat, freestanding circular plate with constant thickness and simply supported

Table 1. Young's modulus [GPa] of interfacial or precipitated Au supracrystals with various NC sizes (Au_5–Au_8).

Type of Supracrystal	Analysis Model	Au_5	Au_6	Au_7	Au_8
Interfacial supracrystals	Plate	0.24 ± 0.18	0.10 ± 0.06	0.09 ± 0.05	0.08 ± 0.04
	Oliver & Pharr	1.10 ± 0.29	0.23 ± 0.07	0.16 ± 0.08	0.11 ± 0.02
Precipitated supracrystals	Oliver & Pharr	5.1 ± 1.4	3.2 ± 0.9	1.8 ± 0.6	0.71 ± 0.38

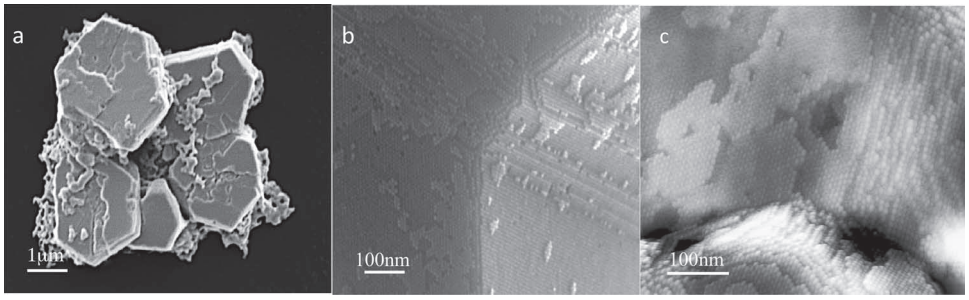

Figure 3. SEM and AFM images of precipitated Au supracrystals. a) SEM image of shaped precipitated supracrystal solids. b) High-magnification SEM image showing different facets of precipitated supracrystals with highly ordered Au NCs and the corresponding AFM image (c).

at its edge. The plate bends downwards under a loading force applied over a small area at the center of the plate. Since the interfacial supracrystals are deposited over the circular holes on the grids, the plate model describes exactly the experimental conditions. The elastic modulus E is then deduced from Equation (2) (see Experimental Section) and the values are listed in Table 1. Similarly to the results of the Oliver and Pharr model, these elastic moduli decrease when the NC size increases, the average E dropping from 240 MPa to 80 MPa. Although the exact values obtained from these two models are different, it is possible to conclude that interfacial supracrystals have soft elastic properties. As explained above, the higher value of E from the Oliver and Pharr model compared to the plate model could be due to the films bending downwards during the indentation, which results in an overestimation of the loading force and thus larger value of E. Since the two models determine the elastic modulus independently, these results confirm that the interfacial supracrystals have E values as low as around 100 MPa. This fact reveals a totally new feature of self-assembled nanocrystals that has never been mentioned before.

Further evidence for such softness of the interfacial supracrystals is the residual mark recorded after the indentation. In Figure 2c, NCs can be clearly observed piled up next to the residual mark, which indicates that individual NCs are squeezed to the surface during the indentation and the interaction between them is weak. This phenomenon has not been reported in previous publications. The third piece of evidence is the discrepancy of the E value between the Oliver and Pharr model and the plate model. From Table 1 it is observed that the discrepancy decreases dramatically as the films become softer from Au_5 to Au_8. For instance, the two methods yield almost the same E value for Au_8 interfacial supracrystals. This could be explained in terms of the Au_8 interfacial supracrystals being so soft that the AFM tip would tend to penetrate into the supracrystal films, causing plastic deformation, rather than press the films into a downward bend, thus resulting in a similar value for the two models. Moreover, to our knowledge, very few studies have focused on the mechanical properties of 100 nm thick supracrystal films and this is the first time that their elastic softness has been stressed. D. Lee and co-workers have reported that 500 nm thick CdSe NC films on solid substrates possess elastic moduli of several gigapascals (using the Oliver and Pharr model).[36] However, the indentation depth in their work was about 200 nm, which is almost 1/3 of the thickness of the films. Thus the substrate effect should have been taken into account in the calculation. Hence, not only the results of the two models, but also the AFM images and the converging elastic modulus discrepancy make us fairly confident that the interfacial supracrystals are unique self-assembled nanomaterials with soft elastic properties (80–240 MPa).

To explore the origin of such softness of interfacial supracrystals, we considered whether it could be attributed to the layer-by-layer growth process, especially since the supracrystals with elastic moduli of several gigapascals are formed in totally different way.[12] In previous studies, the supracrystals, that is, monolayer[30,35] or shaped[12,31] supracrystals, were self-assembled on top of water or glass/ITO (indium tin oxide), respectively, which normally leads to holistic, robust structures as reported. Here, the interfacial supracrystals are formed at the air/solvent interface and the films are floating during the formation, which results in soft layer-by-layer supracrystals. It could be these different growing processes that lead to different mechanical properties. Podsiadlo et al.[12] also showed a difference in the mechanical behavior between evaporated NC films and shaped NC supracrystals in their work, in which the film supracrystals have Young's moduli of several hundred megapascals. These values are close to our results and support the assumption that the growth mechanism affects the mechanical properties. However, their results for film supracrystals are not as small as ours, which is probably due to the difference between evaporation growth and interfacial growth.

2.3. Precipitated Supracrystals

To verify the assumption above, we repeated the nanoindentation measurements on the precipitated supracrystals that formed simultaneously with the interfacial supracrystals from the same batch of NC solution, as described previously. Such precipitated supracrystals are characterized by well-defined shapes ranging in size from 1 μm to 10 μm (**Figure 3**a) and their surfaces are characterized by 2D nucleation without any dislocations (Figure 3b). Moreover, the AFM image (Figure 3c) also reveals the well-defined surface, which, however, is much rougher than that of the interfacial films (Figure 1b).

The mechanical properties of precipitated supracrystals were investigated by nanoindentation measurements (**Figure 4**a) as well, using the Oliver and Pharr model. Here this model

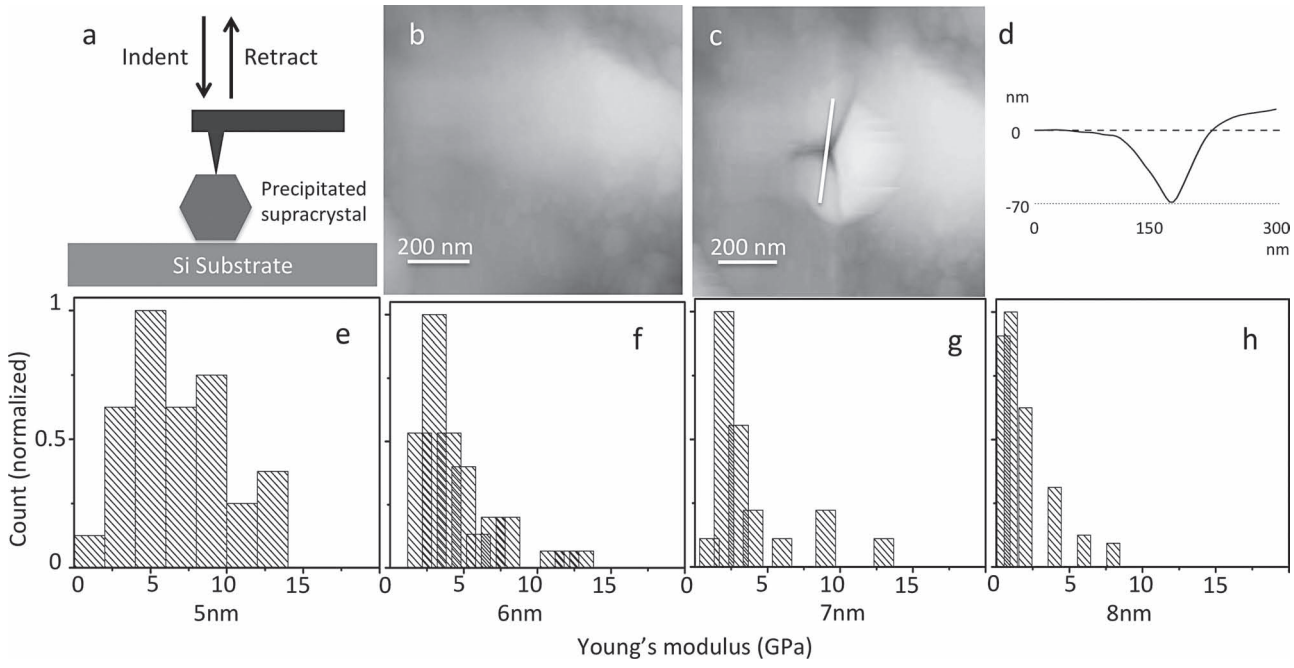

Figure 4. AFM nanoindentation performed on precipitated Au supracrystals. a) Schematic illustration of nanoindentation measurements performed on precipitated supracrystals. b,c) AFM images before (b) and after (c) indentation with residual mark. d) The profile of the residual mark shows a totally different plastic behavior of precipitated supracrystals compared to interfacial ones. e–h) Histogram of Young's modulus obtained from precipitated Au supracrystals with different NC sizes (5 nm, 6 nm, 7 nm, 8 nm)

is suitable because the thickness of precipitated supracrystals (larger than 1 μm) is more than 10 times the indentation depth (about 80 nm). Thus it is reasonable to consider that the substrate does not affect the measurements. The same steps as for the interfacial supracrystals were repeated to extract the Young's modulus for the precipitated supracrystals. AFM images were taken before (Figure 4b) and after (Figure 4c) the indentation as stated above to check its signature. Figure 4d displays the profile of the indentation residual mark (line in Figure 4c), which shows a totally different shape of plastic deformation compared to the interfacial one. Several nanoindentation measurements at different locations were recorded for each sample and supracrystals with various NC sizes were investigated and compared with the counterpart interfacial ones. The corresponding histograms are presented in Figure 4e–h, showing that the average Young's modulus E ranges from 5.1 GPa to 0.71 GPa (Table 1) for different-size Au NCs. The E values obtained for precipitated supracrystals are consistent with the previously mentioned reports on shaped supracrystal aggregates, which are of key importance, revealing that: i) the shaped supracrystals (including our precipitated supracrystals) are characterized by an elastic modulus in the gigapascal range, regardless of the core material (e.g., PbS,[12] CdSe,[31] and Au in our case); ii) when the results for precipitated and interfacial Au supracrystals are compared, it is obvious that the E value of the former is almost one order of magnitude greater than for the latter. This discrepancy is observed for each NC size (from Au_5 to Au_8) and it could be a label to distinguish precipitated and interfacial supracrystals.

According to earlier studies, the reason for a change of Young's modulus of supracrystals could be the degree of NC ordering,[12] the core–ligand interaction,[36] or ligand–ligand interaction.[35] As described previously, both interfacial and precipitated supracrystals are composed of close-packed, highly ordered Au NCs, which rules out the suggestion that the drop in the elastic moduli could be related to the degree of NC ordering. Considering that the interfacial and precipitated supracrystals are produced from the same batch of colloidal solution, the difference in the elastic Young's moduli cannot be due to the ligand–core interactions. Therefore, such a change of elastic moduli can only be attributed to the change of ligand–ligand interactions resulting from the supracrystal growth processes.

A further experiment was performed to test the above assumption. The Au_5 precipitated supracrystals, characterized by an elastic modulus of 5.1 GPa, were re-dissolved in hexane. The colloidal solution shows a well-defined plasmon resonance peak, indicating that the NCs retain their integrity without coalescence. This solution was then slowly evaporated, forming layer-by-layer supracrystal films, and the Young's modulus was then measured. The average values of the elastic Young's modulus deduced from the Oliver and Pharr model and the plate model are 1.1 ± 0.4 GPa and 550 ± 160 MPa, respectively. These values are close to those of interfacial supracrystals (1.1 ± 0.3 GPa and 240 ± 180 MPa, respectively), which verifies the difference between the layer-by-layer films and the shaped supracrystals. The higher value of the evaporated supracrystals could be due to the roughness and defects in the films that result from the evaporation mechanism. In general, the consistency of the two models is a strong evidence that the mechanical properties of the supracrystals can be tuned by changing the supracrystal growth process.

3. Conclusions

The mechanical behaviors of self-assembled Au supracrystals, grown simultaneously at the air/solvent interface and in solution, have been investigated by AFM nanoindentation measurements. The plate model was introduced as a complementary model to the Oliver and Pharr model to analyze freestanding supracrystal films that are several hundred nanometers thick. Both models give small values of tens to hundreds of megapascals for the elastic moduli of layer-by-layer supracrystals. Comparing such results to those for the simultaneously grown, shaped, precipitated supracrystals, it indicated that the mechanical properties are related to the supracrystal growth process, since the Young's modulus increased dramatically, by up to a factor of 20. This assumption is supported by further studies in which Au_5 precipitated supracrystals were re-dissolved and evaporated. The obtained layer-by-layer evaporated supracrystals possess similar elastic properties to the layer-by-layer interfacial supracrystals. This result strongly indicates that the mechanical properties of self-assembled nanocrystals could be tuned by choosing the growing process. To our knowledge, this is the first report in which the softness of self-assembled 3D nanocrystals is stressed and characterized. In addition, since the interfacial supracrystals are of constant thickness and formed at the air/solvent interface, they could be transferred onto a variety of substrates easily, and even with controlled thickness. Considering the novel electronic and optical properties of supracrystal films, such soft mechanical behavior would make them strong candidates for next-generation components or devices in a broad range of applications that require flexible and tunable mechanical properties.

4. Experimental Section

Au Nanocrystal Synthesis: The synthesis of Au NCs differing in size is described elsewhere.[32] Briefly, for the synthesis of 8 nm Au nanocrystals, 0.25 mmol of chlorotriphenylphosphine Au(I) was dissolved in toluene (25 mL) then dodecanethiol (125 µL) was added. Next, the mixture was placed in a silicon bath at 100 °C until it became a dark red color. Then this colloidal solution was dried in a nitrogen flow and ethanol was added to the remaining dark powder. After stirring, the solution was centrifuged. After the supernatant had been removed, the black precipitate was dried under nitrogen flow. The black precipitate was the Au nanocrystals and could be purified by repeating the re-dissolving (in toluene)/blow-drying procedure. The size distribution of 8 nm nanocrystals was 6%. The NCs corresponding to this synthesis were denoted by Au_8. By varying the amount of dodecanethiol from 125 µL to 250 µL or 500 µL, Au_7 and Au_6 could be obtained (with size distribution of 7% and 8%, respectively). For the preparation of Au_5, 5 mmol of *tert*-butylamine borane complex dissolved in 2 mL of toluene was used instead of dodecanethiol, while the other procedures were exactly the same. The size distribution of Au_5 was 8%.

Equipment: SEM images were obtained using a JEOL JSM-5510LV, and the high-resolution SEM images were recorded on a Hitachi SU-70. All AFM experiments were performed with a commercial AFM 5100 System (Agilent Technologies, USA) and the probes were provided by MikroMasch with typical spring constant around 4.5 N m^{-1}. The AFM was used in the acoustic mode for image recording and in contact mode for nanoindentation measurements. AFM images were recorded both before and after the indentation to check the nanoindentation residual marks. Several spots were selected randomly for each sample. Protein Unfolding and Nano-Indentation Analysis Software (PUNIAS) was used to perform the Oliver and Pharr indentation analysis.

The Use of AFM as a Nanoindentation Tool: To determine the Young's modulus for each sample, a number of distinct places were selected randomly to perform the indentation, and for each indentation place, an increasing loading force was applied and recorded to track the variation of Young's modulus according to the indentation depth. In the case of freestanding supracrystal films over holes on a TEM grid, a number of fully covered holes were selected on which to perform the indentation. Immediately after each set of measurements, the cantilever was calibrated on a mica substrate to obtain the actual deflection sensitivity and force constant for the elastic modulus calculation. For the calculations using the Oliver and Pharr model, the value of E for each sample was obtained by using the commercial software PUNIAS, which reads the original data, that is, the load–displacement curves, and calculates the Young's modulus by extracting the force versus penetration (*P*–*h*) curve. To specify the contact area between the tip and the sample, the manufacturer's specifications of the tip and the residual marks after the indentation were taken into account, and the shape of the AFM probe was checked using SEM as well. Furthermore, the methodology was verified by measuring the Young's modulus of a reference Teflon foil sample. For the plate model, the contact area was not a parameter for calculation. The displacement of the central point is calculated. The AFM probe used for nanoindentation had a spring constant of 4.5 N m^{-1}.

During the experiments, uniform loadings were not systematically present, which was due to the geometry of the AFM probe. Thus the following steps were taken to verify the data:

1) The results between the uniform loads and non-uniform loads were compared, which showed a very small difference (within the uncertainty region). It was assumed that this was due to the loading area being very small compared to the overall region of the freestanding films. The plate model calculates the behavior of the whole film (the displacement of the center point of the film), thus the local difference is not crucial for the final results.

2) To improve the accuracy of the results, the number of measurements was increased, as was done for the Oliver and Pharr model, to reduce the systematic errors.

Nanoindentation Measurements: *Oliver and Pharr Model*: The elastic modulus of the precipitated supracrystals was determined from the load–displacement curves by applying the Oliver and Pharr model.[37] In this model, the Young's modulus is calculated from

$$E_r = \frac{\sqrt{\pi}}{2}\frac{S}{\sqrt{A}} \quad (1)$$

where E_r is the "reduced modulus", A the projected area of elastic contact, and S the experimentally measured contact stiffness, which is the slope of the initial unloading curve (Figure S2, Supporting Information).

Plate Model: For exploring the mechanical properties of interfacial supracrystals on the TEM grid, the Oliver and Pharr model may not be ideal as the films have limited thickness and they may bend over as a whole under the pressure of the AFM tip. On the other hand, such films cannot be treated as thin films as in previous studies.[34] Thus, a plate model[38] was used to calculate the Young's modulus of interfacial supracrystals and compared to the Oliver and Pharr model.

The plate model treats the interfacial supracrystal film as a flat circular plate with constant thickness. The indentation of the AFM tip was modeled as a uniform load over a very small central circular area and the edge of the plate (the interfacial films) is simply supported (Figure S3, Supporting Information). Then the Young's modulus could be calculated from

$$E = \frac{3Wa^2}{4\pi\gamma t^3}(1-\nu)(3+\nu) \quad (2)$$

where E is the Young's modulus, W the total applied load (force), a the radius of the plate, ν Poisson's ratio, γ the displacement of the central point, and t the thickness of the plate.

Why the Plate Model Could Be the Best to Study Films That Are Several Hundred Nanometers Thick: Although nanoindentation is widely used for the measurements of Young's modulus of nanomaterials, it remains difficult to choose the proper model for analysis of specific materials. Nanocrystal films that are several hundred nanometers thick are good examples. They cannot be deposited onto solid substrates (such as Si or highly ordered pyrolytic graphite (HOPG)) or tested directly because such an approach will cause a huge systematic error resulting from the substrate. One solution is to fabricate freestanding films, which have been already used for the analysis of monolayer or thin films of nanoparticles.[30,34,35] However, the "membrane model" used in those studies is not suitable here, as the ratio between film thickness and hole diameter is much larger than the criterion of the model. Meanwhile, the widely used Oliver and Pharr model is not suitable either, as it requires an infinite (or quasi-infinite) thickness of the investigated object. Hence, the "plate model" is introduced, which allows relatively large film thickness/hole diameter ratio and avoids the effects from the substrate. Furthermore, it fully describes the physical condition of freestanding Au supracrystal films: the films are simply supported by the edge of the circular hole without any sticking or hinging, and the films bend downwards under loading over a small central circular area. Therefore, choosing the plate model is fully due to the special geometrical properties of Au supracrystal films, whose thickness lies between that of membranes and thick aggregates. Although it may not be the most accurate model to be applied, it seems reasonable to conclude that the plate model is the most suitable one so far for the analysis of freestanding films with thickness of several hundred nanometers.

Supporting Information

Supporting Information is available from the Wiley Online Library or from the author.

Acknowledgements

The authors thank Dr. Pierre-Antoine Albouy (Université Paris-Sud 11) for fruitful discussions. The research leading to these results received funding from the European Community's Seventh Framework Programme (FP7/2008-2011) under Grant Agreement no. 213382. The research leading to this paper was partially supported by an Advanced Grant of the European Research Council under Grant Agreement no. 267129.

Received: September 6, 2012
Published online: January 9, 2013

[1] L. Motte, F. Billoudet, M. P. Pileni, *J. Phys. Chem.* **1995**, *99*, 16425.
[2] C. B. Murray, C. R. Kagan, M. G. Bawendi, *Science* **1995**, *270*, 1335.
[3] S. A. Harfenist, Z. L. Wang, R. L. Whetten, I. Vezmar, M. M. Alvarez, *Adv. Mater.* **1997**, *9*, 817.
[4] C. P. Collier, T. Vossmeyer, J. R. Heath, *Annu. Rev. Phys. Chem.* **1998**, *49*, 371.
[5] B. A. Korgel, D. Fitzmaurice, *Adv. Mater.* **1998**, *10*, 661.
[6] R. L. Whetten, M. N. Shafigullin, J. T. Khoury, T. G. Schaaff, I. Vezmar, M. M. Alvarez, A. Wilkinson, *Acc. Chem. Res.* **1999**, *32*, 397.
[7] M. P. Pileni, *J. Phys. Chem. B* **2001**, *105*, 3358.
[8] S. I. Stoeva, B. L. V. Prasad, S. Uma, P. K. Stoimenov, V. Zaikovski, C. M. Sorensen, K. J. Klabunde, *J. Phys. Chem. B* **2003**, *107*, 7441.
[9] A. Courty, A. Mermet, P. A. Albouy, E. Duval, M. P. Pileni, *Nat. Mater.* **2005**, *4*, 395.
[10] M. P. Pileni, *Acc. Chem. Res.* **2007**, *40*, 685.
[11] M. P. Pileni, *Acc. Chem. Res.* **2008**, *41*, 1799.
[12] P. Podsiadlo, G. Krylova, B. Lee, K. Critchley, D. J. Gosztola, D. V. Talapin, P. D. Ashby, E. V. Shevchenko, *J. Am. Chem. Soc.* **2010**, *132*, 8953.
[13] D. V. Talapin, E. V. Shevchenko, C. B. Murray, A. V. Titov, P. Kral, *Nano Lett.* **2007**, *7*, 1213.
[14] I. Lisiecki, V. Halte, C. Petit, M. P. Pileni, J. Y. Bigot, *Adv. Mater.* **2008**, *20*, 4176.
[15] N. Zaitseva, Z. R. Dai, F. R. Leon, D. Krol, *J. Am. Chem. Soc.* **2005**, *127*, 10221.
[16] E. V. Shevchenko, D. V. Talapin, S. O'Brien, C. B. Murray, *J. Am. Chem. Soc.* **2005**, *127*, 8741.
[17] D. V. Talapin, C. B. Murray, *Science* **2005**, *310*, 86.
[18] H. Fudouzi, Y. N. Xia, *Langmuir* **2003**, *19*, 9653.
[19] C. R. Kagan, C. B. Murray, M. G. Bawendi, *Phys. Rev. B* **1996**, *54*, 8633.
[20] Z. H. Nie, A. Petukhova, E. Kumacheva, *Nat. Nanotechnol.* **2010**, *5*, 15.
[21] A. R. Tao, D. P. Ceperley, P. Sinsermsuksakul, A. R. Neureuther, P. D. Yang, *Nano Lett.* **2008**, *8*, 4033.
[22] E. V. Shevchenko, D. V. Talapin, N. A. Kotov, S. O'Brien, C. B. Murray, *Nature* **2006**, *439*, 55.
[23] C. Sire, F. Ardiaca, S. Lepilliet, J. W. Seo, M. C. Hersam, G. Dambrine, H. Happy, V. Derycke, *Nano Lett.* **2012**, *12*, 1184.
[24] C. Wang, J. C. Chien, K. Takei, T. Takahashi, J. Nah, A. M. Niknejad, A. Javey, *Nano Lett.* **2012**, *12*, 1527.
[25] R. J. Knuesel, H. O. Jacobs, *Proc. Natl. Acad. Sci. USA* **2010**, *107*, 993.
[26] V. Germain, M. P. Pileni, *Adv. Mater.* **2005**, *17*, 1424.
[27] R. Li, L. H. Bao, X. D. Li, *CrystEngComm* **2011**, *13*, 5858.
[28] P. Jiang, J. J. Zhou, R. Li, Z. L. Wang, S. S. Xie, *Nanotechnology* **2006**, *17*, 3533.
[29] N. Goubet, H. Portales, C. Yan, I. Arfaoui, P. A. Albouy, A. Mermet, M. P. Pileni, *J. Am. Chem. Soc.* **2012**, *134*, 3714.
[30] K. E. Mueggenburg, X. M. Lin, R. H. Goldsmith, H. M. Jaeger, *Nat. Mater.* **2007**, *6*, 656.
[31] E. Tam, P. Podsiadlo, E. Shevchenko, D. F. Ogletree, M. P. Delplancke-Ogletree, P. D. Ashby, *Nano Lett.* **2010**, *10*, 2363.
[32] N. Goubet, J. Richardi, P. A. Albouy, M. P. Pileni, *Adv. Funct. Mater.* **2011**, *21*, 2693.
[33] T. Chudoba, N. Schwarzer, F. Richter, *Surf. Coat. Technol.* **2000**, *127*, 9.
[34] H. L. Qin, J. Jin, X. S. Peng, I. Ichinose, *J. Mater. Chem.* **2010**, *20*, 858.
[35] J. B. He, P. Kanjanaboos, N. L. Frazer, A. Weis, X. M. Lin, H. M. Jaeger, *Small* **2010**, *6*, 1449.
[36] D. Lee, S. G. Jia, S. Banerjee, J. Bevk, I. P. Herman, J. W. Kysar, *Phys. Rev. Lett.* **2007**, *98*, 026103.
[37] W. C. Oliver, G. M. Pharr, *J. Mater. Res.* **1992**, *7*, 1564.
[38] W. C. Young, R. G. Budynas, *Roark's Formulas for Stress and Strain*, McGraw-Hill, New York **2002**.